1-26-2017

Neurovascular Astrocyte Degeneration in the Hyperhomocysteinemia Model of Vascular Cognitive Impairment and Dementia (VCID)

Tiffany L. Sudduth
University of Kentucky, tlsudd2@uky.edu

Erica M. Weekman
University of Kentucky, emweek2@uky.edu

Brittani Rae Price
University of Kentucky, brpr222@g.uky.edu

Jennifer L. Gooch
University of Kentucky, jenn.gooch@uky.edu

Abigail E. Woolums
University of Kentucky, abigail.woolums@uky.edu

Neurovascular Astrocyte Degeneration in the Hyperhomocysteinemia Model of Vascular Cognitive Impairment and Dementia (VCID)

Digital Object Identifier (DOI)
https://doi.org/10.1016/j.neuroscience.2016.11.024

Notes/Citation Information
Published in *Neuroscience*, v. 341, p. 42-51.

Authors
Tiffany L. Sudduth, Erica M. Weekman, Brittani Rae Price, Jennifer L. Gooch, Abigail E. Woolums, Christopher M. Norris, and Donna M. Wilcock

Published in final edited form as:

Neuroscience. 2017 January 26; 341: 42–51. doi:10.1016/j.neuroscience.2016.11.024.

Neurovascular astrocyte degeneration in the hyperhomocysteinemia model of vascular cognitive impairment and dementia (VCID)

Tiffany L. Sudduth[1], **Erica M. Weekman**[1,2], **Jennifer L. Gooch**[1,2], **Abigail Woolums**[1], **Christopher M. Norris**[1,3], and **Donna M. Wilcock**[1,2,*]

[1]University of Kentucky, Sanders-Brown Center on Aging, Lexington, KY 40536 USA

[2]University of Kentucky, Department of Physiology, Lexington, KY 40536 USA

[3]University of Kentucky, Department of Pharmacology and Nutritional Sciences, Lexington, KY 40536 USA

Abstract

Vascular cognitive impairment and dementia (VCID) is the second leading cause of dementia behind Alzheimer's disease (AD) and is a frequent co-morbidity with AD. Despite its prevalence, little is known about the molecular mechanisms underlying the cognitive dysfunction resulting from cerebrovascular disease. Astrocytic end-feet almost completely surround intraparenchymal blood vessels in the brain and express a variety of channels and markers indicative of their specialized functions in the maintenance of ionic and osmotic homeostasis and gliovascular signaling. These functions are mediated by end-foot enrichment of the aquaporin 4 water channel (AQP4), the inward rectifying potassium channel Kir4.1 and the calcium-dependent potassium channel MaxiK.

Using our HHcy model of VCID we examined the time-course of astrocytic end-foot changes along with cognitive and neuroinflammatory outcomes. We found that there were significant astrocytic end-foot disruptions in the HHcy model. AQP4 becomes dislocalized from the end-feet, there is a loss of Kir4.1 and MaxiK protein expression, as well as a loss of the Dp71 protein known to anchor the Kir4.1, MaxiK and AQP4 channels to the end-foot membrane. Neuroinflammation occurs prior to the astrocytic changes, while cognitive impairment continues to decline with the exacerbation of the astrocytic changes.

We have previously reported similar astrocytic changes in models of cerebral amyloid angiopathy (CAA) and therefore, we believe astrocytic end-foot disruption could represent a common cellular mechanism of VCID and may be a target for therapeutic development.

Keywords

Neuroinflammation; astrocyte; dementia; cerebrovascular; microhemorrhage

*To whom correspondence should be addressed: Donna M. Wilcock, PhD, University of Kentucky, Room 424 Sanders-Brown Center on Aging, 800 S Limestone St, Lexington, KY 40536, USA, donna.wilcock@uky.edu, Tel: +1 859 218 2390, Fax: +1 859 323 2866.

Introduction

Vascular contribution to cognitive impairment and dementia (VCID) is widely considered to be the second most common cause of dementia after Alzheimer's disease (AD), accounting for 20–30 percent of cases (Levine and Langa, 2011). In addition, VCID occurs as a co-morbidity with other common dementias including AD, where it is estimated to occur in as many as 40% of all cases (Bowler et al., 1998, Kammoun et al., 2000, Langa et al., 2004, Snyder et al., 2015). Over twenty years ago, hyperhomocysteinemia (HHcy) was identified as an independent risk factor for stroke and vascular disease (Refsum et al., 1998). HHcy is also associated with pathologically-confirmed VCID and AD (Clarke et al., 1998) and is now accepted as a risk factor for AD (Beydoun et al., 2014). We have established a hyperhomocysteinemia (HHcy) model of VCID in wildtype, C57BL6, mice. Dietary induction of HHcy is achieved by the elimination of B6, B12 and folate from the diet and enrichment with methionine (Troen et al., 2008). The mice develop cognitive impairment, cerebral microhemorrhages and neuroinflammation in response to the diet (Sudduth et al., 2013).

Astrocytes compose 50% of the cells of the brain and play several key roles in maintaining the health of the neurons. In particular, they buffer potassium to regulate the excitability of the neurons (Newman et al., 1984, Simard and Nedergaard, 2004, Wallraff et al., 2006). This potassium buffering is also thought to contribute, at least in part, to the process of neurovascular coupling; i.e., the process of matching local cerebral blood flow to the local neuronal activity (Dunn and Nelson, 2010, Witthoft et al., 2013), however, the potassium buffering role in neurovascular coupling remains disputed (Metea et al., 2007). To perform the critical function of potassium buffering and osmotic homeostasis, astrocytes ensheath the cerebrovasculature with specialized processes called end-feet. The astrocytic end-feet express a variety of channels and markers indicative of their specialized functions in the maintenance of ionic and osmotic homeostasis and gliovascular signaling (Simard and Nedergaard, 2004). The channels enriched at the astrocytic end-feet are the aquaporin 4 water channel (AQP4) (Amiry-Moghaddam et al., 2003), the inward rectifying potassium channel Kir4.1 (Butt and Kalsi, 2006) and the calcium-dependent potassium channel MaxiK (also known as the BK channel) (Price et al., 2002). AQP4 and Kir4.1 are almost exclusively expressed by astrocytic end-feet (Simard and Nedergaard, 2004). The MaxiK channel is primarily in the astrocytic end-feet, with some expression by astrocyte processes that are not associated with the vasculature (Farr and David, 2011).

We have previously shown that cererbral amyloid angiopathy (CAA) results in AQP4 dislocalization from the astrocytic end-foot, and loss of Kir4.1 and MaxiK channels. These findings were observed in both the APPSwDI mouse model of CAA and human AD with high CAA (Wilcock et al., 2009). In the current study we examine the astrocytic end-foot markers in our HHcy mouse model of VCID along a time-course. We find that astrocytic end-feet are significantly disrupted in the HHcy model. These changes are not apparent after 6 weeks of HHcy induction, but are after 10 weeks, and are significantly worse after 14 weeks of induction. Along a similar time-course, cognitive impairment is not observed until 10 weeks after HHcy induction, and performance is worse 14 weeks after HHcy induction.

Materials and Methods

Animals

Seventy-two C57BL6 wildtype mice aged 3 months were placed on diet with low levels of folate, vitamins B6 and B12 and enriched with methionine (N=12/time-point) (Harlan Teklad TD97345; Harlan Teklad, Madison, WI) or a control diet that nutritionally matched the experimental diet with normal levels of methionine, folate, vitamins B6 and B12 (N=12/time-point) (Harlan Teklad 5001C; Harlan Teklad, Madison, WI). Mice received diet for 6, 10 and 14 weeks. Mice were weighed weekly to ensure no significant malnourishment was occurring due to the diet. The study was approved by the University of Kentucky Institutional Animal Care and Use Committee and conformed to the National Institutes of Health Guide for the Care and Use of Animals in Research.

Behavior testing

The two-day radial-arm water maze protocol was performed during the week prior to tissue harvest as previously published (Alamed et al., 2006). Briefly, a six-arm maze was submerged in a pool of water, and a platform was placed at the end of one arm (equipment and tracking software from Noldus Information Technology Inc., Leesburg VA). Each mouse received 15 trials per day for 2 days. The mouse began each trial in a different arm while the arm containing the platform remained the same. The numbers of errors (incorrect arm entries) were counted over a one-minute period. The errors were averaged over three trials, resulting in 10 blocks for the two-day period (blocks 1–5 are day 1 while blocks 6–10 are day 2).

Tissue processing and histology

After injection with a lethal dose of beuthanasia-D, blood was collected for plasma and the mice were perfused intracardially with 25ml normal saline. Brains were rapidly removed and bisected in the mid-sagittal plane. The left half was immersion fixed in 4% paraformaldehyde for 24 hours, while the right half was dissected into anterior cerebral cortex, posterior cerebral cortex, striatum, hippocampus, thalamus, cerebellum and rest of brain. The posterior cerebral cortex and rest of brain were combined and immediately homogenized in PBS for zymography (see detailed method below). The remaining pieces were flash frozen in liquid nitrogen and stored at −80°C. The left hemibrain was passed through a series of 10, 20 and 30% sucrose solutions as cryoprotection and 25μm frozen horizontal sections were collected serially using a sliding microtome and stored floating in PBS containing sodium azide at 4°C. Plasma samples were analyzed for Hcy levels by the clinical laboratories of the University of Kentucky.

Eight sections equally spaced 600mm apart were selected for free floating immunohistochemistry for GFAP (Rat anti-GFAP, clone 2.2B10; Invitrogen, Camarillo, CA; 1:3,000), AQP4 (Rabbit polyclonal anti-AQP4; Millipore, Temecula, CA; 1:5,000) and Dp71 (Rabbit polyclonal anti-dystrophin 1, cross-reacting with Dp71; Abcam, Cambridge MA; 1:3,000). The method for free-floating immunohistochemistry has been described previously (Wilcock et al., 2008). Sixteen sections equally spaced 300mm apart were mounted on slides and stained for Prussian blue as described previously (Wilcock et al., 2004).

Quantitative real-time RT-PCR

RNA was extracted from the right hippocampus using the E.Z.N.A. Total RNA kit (Omega Bio-Tek, Norcross, GA, USA) according to the manufacturer's instructions. RNA was quantified using the Biospec nano spectrophotometer (Shimaduz, Japan). cDNA was produced using the cDNA High Capacity kit (ThermoFisher, Grand Island, NY, USA) according to the manufacturer's instructions. Real-time PCR was performed using the Fast TaqMan Gene Expression assay (ThermoFisher, Grand Island, NY, USA). In each well of a 96-well plate, 0.5μL cDNA (100ng, based on the RNA concentrations) was diluted with 6.5μL RNase-free water. One microliter of the appropriate gene probe was added along with 10μL of Fast TaqMan to each well. Target amplification was performed using the ViiA7 (Applied Biosystems, Grand Island, NY, USA). All genes were normalized to 18S rRNA and the fold change was determined using the $-\Delta\Delta Ct$ method (Livak and Schmittgen, 2001).

Western Blot

Approximately 60mg of the brain powder was homogenized and protein lysates were prepared in M-per lysis buffer (Thermo Scientific, Rockford, IL) containing 1% complete protease/phosphatase inhibitor (Thermo Scientific, Rockford IL). Protein concentrations were assessed using the BCA protein assay kit (Thermo Scientific, Rockford, IL), according to manufacturer's instructions. 15μg protein from each lysate was run on a denaturing 4–20% SDS-PAGE gel. The gel was transferred onto a PVDF membrane using the iBlot system (Invitrogen, Carlsbad CA), and Western blots were performed for Kir4.1 (Rabbit polyclonal anti-Kir4.1; Millipore, Temcula, CA; 1:3,000) and MaxiK (Rabbit polyclonal anti-MaxiK channel; Bioss, Wolburn, MA; 1:500). The blots were stripped using 5X New Blot Nitro Stripping Buffer (Licor, Lincoln NE) and re-probed using the above protocol for with β-actin as loading control (Rabbit monoclonal anti-b-actin, clone 13E5; Cell Signaling Technology, Danvers, MA; 1:10,000). Semi-quantitative densitometry analysis was performed using the Odyssey Imaging Software (Licor, Lincoln, NE). Individual densitometry values were normalized to the β-actin densitometry value on the same blot.

Image analysis

Individuals who were blinded to the study, treatment groups and genotype of the animals performed the image analysis. Images were collected using the Zeiss AxioScan slide scanner. Frontal cortex and hippocampus were outlined maintaining uniformity through the use of neuroanatomical landmarks. Eight sections for frontal cortex and between four and six sections for hippocampus were analyzed per animal. To assess astrogliosis and microgliosis, we examined frontal cortex, and the hippocampus for percent area occupied by positive stain was analyzed using the Elements AR Image Analysis System (Nikon Instruments, Melville, NY). To assess AQP4 and Dp71 staining, we counted the numbers of vessels per region. A blinded investigator collected images in the same way as above, however, this time, numbers of vessels were counted by manually clicking on vessels using the same image analysis system. Eight sections for frontal cortex and 4–6 sections for hippocampus were analyzed per animal.

Statistical analysis

Data are presented as mean ± standard error of mean (SEM). Statistical analysis was performed using the JMP statistical analysis program (SAS, Cary NC). Radial-arm water maze data and rotarod was analyzed by repeated measures ANOVA to assess overall effect of diet. For the radial-arm water maze data, we also performed student's t-test on individual block data. For other data, one-way ANOVA and student's t test were performed. Statistical significance was assigned where the P-value was lower than 0.05.

Results

Elevated Hcy levels were achieved in all groups with no significant difference between the 6, 10 and 14 weeks on diet. The levels ranged from 60–105μmol/L with no difference between any of the HHcy groups. The mice receiving the control diet all came in below the detection range of the clinical laboratory assay, which is also a finding on the normal mouse chow of our animal facilities. The two-day radial-arm water maze was performed immediately prior to sacrifice. All mice, regardless of diet administration or duration of diet administration, began the two days of testing making a high number of errors, as expected given all mice were naïve to the task (figure 1A–C). After 6 weeks on diet, the HHcy and control mice were virtually indistinguishable with the exception of block 8, where the HHcy mice made significantly more errors than the control mice (figure 1A). Following 10 weeks of diet administration, there are clear deficits in the two-day radial-arm water maze. The deficits are mostly apparent on the second day. On the first block of day 2, the HHcy mice make significantly more errors than the control mice, indicating a lack of consolidation between days. Further, by the end of the second day the HHcy mice are still making significantly more errors than the control mice (figure 1B). After 14 weeks of diet administration, HHcy mice are significantly impaired across both days 1 and 2, indicating impairment in both acquisition and consolidation (figure 1C).

We have previously shown that HHcy results in significant cerebrovascular pathology, as evidenced by the occurrence of multiple microhemorrhages (Sudduth et al., 2013). In the current study we find that microhemorrhage occurrence is dependent on duration of diet administration. Microhemorrhages are apparent after only 6 weeks of diet administration, but this is increased and shows statistical significance with 10 weeks of diet administration. There is a further significant increase after 14 weeks of diet administration (figure 2). Across the time-course of the current study we do not see any increase in the apparent size of the microhemorrhages, but rather their numbers (examples of microhemorrhages are shown in the images of figure 2).

In the current study, we focused on the astrocytes of the neurovascular unit, in particular, any changes in the astrocytic end-foot markers that may indicate a dysfunctional neurovascular unit. We first examined astrocytes by performing GFAP immunohistochemistry. There is no apparent astrogliosis in response to HHcy, even after 14 weeks following diet administration, where we see significant cerebrovascular pathology (figure 3).

AQP4 is a passive water channel that is highly polarized to the astrocytic end-foot. Immunolabeling for AQP4 shows cerebrovascular labeling throughout the brain. Figure 4

shows representative images of AQP4 immunolabeling of the frontal cortex of 14 weeks of control diet administration (figure 4), or 6, 10 and 14 weeks of HHcy inducing diet administration (figure 4). It is clear from the images that there is a decrease in AQP4 labeling of blood vessels with increasing duration of HHcy induction. We quantified the numbers of AQP4 positive vessels immunolabeled. As can be seen from figure 4E, there is no significant difference between control and HHcy with 6 weeks of diet administration, however, AQP4 positive vessels are decreased in the frontal cortex and CA3 region of the hippocampus of HHcy mice compared to control mice after 10 weeks of diet administration. These same changes are apparent with 14 weeks of diet administration, however there is also a significant decrease in AQP4 positive vessels in the CA1 region of the hippocampus as well as the CA3 and the frontal cortex with 14 weeks of diet administration.

The Dp71 short form of dystrophin 1 is known as a key anchoring protein for the AQP4 channel (Connors and Kofuji, 2002, Amiry-Moghaddam et al., 2003). Immunolabeling for Dp71 shows the same distribution as AQP4, with labeling of cerebral blood vessels (Figure 5). In mice on control diet for 14 weeks, there are numerous blood vessels labeled for Dp71 throughout the brain (frontal cortex shown in figure 5). Six weeks of diet administration to induce HHcy does not significantly alter Dp71 expression as detected by immunolabeling (figure 5). However, we found a significant decrease in blood vessel labeling with Dp71 after both 10 and 14 weeks of diet administration to induce HHcy (figure 5).

Co-anchored with the AQP4 channel, are the potassium channels Kir4.1 and the MaxiK channel. These channels are crucial to the astrocyte function of potassium buffering. We have quantified both the mRNA and protein levels of these two channels in the current study. We found that gene expression levels of Kir4.1 were unchanged with 6 weeks of diet, but decreased with 10 and 14 weeks of diet administration to induce HHcy (figure 6A). Similarly, levels of MaxiK gene expression were also decreased at the 10 and 14-week time points, but an intriguing significant increase in gene expression occurred at the 6-week time-point (figure 6A). However, we observed an increase in MaxiK gene expression following 6 weeks of diet administration to induce HHcy (figure 6A). Protein expression of Kir4.1 and MaxiK, as assessed by Western blot, showed similar reductions in expression with 10 and 14 weeks of diet administration to induce HHcy, but there was no change with only 6 weeks of diet administration. The increase at the 6 week time-point in MaxiK gene expression did not translate to an increase in protein expression (figure 6B and C).

Neuroinflammation is another phenomenon observed in our HHcy model. Microglial activation, as measured by CD11b immunohistochemistry, is observed in HHcy mice and this increase remains across all time-points examined, with no difference between the three time-points studied (Figure 7). Pro-inflammatory mediators IL-1β, IL-6, IL-12 and TNFα are all significantly increased in our HHcy model at all time-points studied (Figure 8). However, the time-course of each is different. TNFα shows a steady state increase across all time-points. However, IL-1β increases gradually over the time-points studied. IL-6 increased quite sharply between the 10 and 14-week time-points. IL-12 appears to peak at the 10 week time-point, however, due to the high variability there was no difference between any of the time-points.

Discussion

VCID is the second most common cause of dementia behind AD. More critically, VCID is also a frequent co-morbidity in sporadic AD cases, and also other dementias. Studies on VCID have been hindered by the lack of animal models to study mechanistic underpinnings of the vascular contribution to dementia. We have previously shown that CAA pathology is associated with astrocytic end-foot dysfunction in AD and in CAA mouse models (Wilcock et al., 2009). We hypothesized that astrocytic end-foot dysfunction may also be a key pathological process in VCID. To test this we performed a time-course study in our HHcy mouse model of VCID. This model reproduces aspects of VCID including neuroinflammation, cognitive impairment and blood-brain barrier breakdown culminating in microhemorrhages throughout the cerebral cortex and, less frequently, hippocampus (Sudduth et al., 2013). In the current study, we examined mice on HHcy-inducing diet for a period of 6, 10 and 14 weeks. We then did a careful histological and biochemical assessment of astrocytic end-foot markers, as well as behavior and neuroinflammation.

The cererbovasculature of the brain, primarily arterioles and capillaries, are almost completely ensheathed by astrocytic processes called astrocytic end-feet. The astrocytic end-foot is a specialized unit that functions to maintain the ionic and osmotic homeostasis of the brain. To perform this function, the end-feet are enriched with aquaporin 4 (AQP4) water channels, as well as the potassium channels Kir4.1 and MaxiK (Newman et al., 1984, Simard and Nedergaard, 2004, Bay and Butt, 2012). The anchoring proteins responsible for maintaining these channels in the end-foot are the syntrophin-dystrophin 1 complex (Connors and Kofuji, 2002, Amiry-Moghaddam et al., 2003, Amiry-Moghaddam et al., 2004a, Amiry-Moghaddam et al., 2004b, Camassa et al., 2015). In the current study, HHcy diet mice showed a reduction in DP71 labeling concurrent with reduced vascular labeling for AQP4, and lower protein/mRNA levels for Kir4.1 and MaxiK potassium channels. These observations suggest that HHcy leads to astrocyte end-feet disruption, which is likely to have significant implications for both potassium homeostasis and neurovascular coupling.

The astrocytic end-foot is anchored to the vascular basement membranes via the α-β dystroglycan complex (Noell et al., 2011, Gondo et al., 2014). Matrix metalloproteinase 9 (MMP9) (Michaluk et al., 2007), which shows high expression levels in astrocytes (ref?*), appears to be a major degrading enzyme of the dystroglycans, specifically β-dystroglycan. Because MMP9 is regulated through the neuroinflammatory response we examined the neuroinflammatory state of the HHcy mice. We found microglial activation, as assessed by CD11b immunohistochemistry, at all time-points examined, including the earliest, 6-week time-point. While microglial activation remains elevated and steady across the time-course studied, we found that the expression of pro-inflammatory mediators had different time-courses of changes. IL-1β and TNFα are known to be the primary regulators of MMP9 expression (Chakrabarti et al., 2006, Loesch et al., 2010, Klein and Bischoff, 2011). We found that TNFα expression peaks at the earliest time-point examined; 6 weeks. While there was a slight decline at the 10 and 14-week time-points, these changes were not significantly lower than the 6-week expression and remained significantly elevated compared to the mice on control diet. IL-1b showed a steady increase in expression over the time-course, with a modest increase at the 6-week time-point, a significant increase at the 10 week time-point

and a further increase at the 12-week time-point. Both IL-12 and IL-6 were also significantly increased as a result of HHcy at all time-points examined. These data are consistent with our previous reports of induction of a pro-inflammatory state by HHcy (Sudduth et al., 2013, Sudduth et al., 2014). Given that neuroinflammation precedes the astrocytic changes and cerebrovascular pathology it is possible that neuroinflammatory responses are key mediators of these later pathologies.

When we assessed cognition using the two-day radial water maze test of spatial memory, we found that significant impairment was only apparent at the 10 and 14-week time-points, with only one block of trials showing a deficit in the 6-week time-point. We can therefore conclude that the presence of neuroinflammation alone, in the absence of cerebrovascular/astrocyte pathologies or other changes we have examined, is insufficient to induce a significant cognitive impairment. Only when other pathological events occur, specifically microhemorrhages and astrocytic end-feet degeneration, do we see cognitive impairment. While neuroinflammatory changes have been associated with cognitive impairment in the past, this has typically been associated with sub-chronic administration of the potent immune stimulator lipopolysaccharide (Semmler et al., 2007, Czerniawski et al., 2015, Sun et al., 2015). The HHcy diet does not appear to generate as robust an inflammatory response as that seen with LPS. However, based on our observations, we hypothesize that astrocytic end-foot degeneration and blood-brain barrier leakage are downstream consequences of the inflammatory response, and proximal causes of cognitive impairment.

Potassium buffering is a key function of the astrocyte, and the astrocytic expression of Kir4.1 and AQP4 at the end-foot is considered a critical component of this function. It has been shown that deletion of the KCNJ10 gene, (Kir4.1), results in impaired potassium buffering after synaptic activation and is associated with epilepsy (Haj-Yasein et al., 2011, Larsen and MacAulay, 2014). AQP4 deletion is also associated with impaired potassium buffering, likely through the altered osmotic balance (Strohschein et al., 2011). Cognitive impairment worsens with increasing time on the HHcy-inducing diet. Only when the astrocytic end-foot changes are present do we observe significant cognitive impairment in the two-day radial arm water maze. We predict that it is impaired potassium buffering that is mediating the cognitive impairment in the HHcy mouse model.

In conclusion, our HHcy model of VCID shows significant astrocytic end-foot degeneration including loss of the Dp71 anchoring protein, dislocalization of the AQP4 channel, and decreased expression of the two key potassium channels Kir4.1 and MaxiK. These events occur at the same time as cerebrovascular pathology is present. These events are preceded in the time-course by a pro-inflammatory response in the brain and microglial activation. Despite the early inflammatory response, cognitive impairment is only apparent when we find astrocytic end-foot changes and cerebrovascular pathology. Intriguingly, the same astrocytic changes were previously reported by ourselves in the CAA mouse model and in human AD with CAA (Wilcock et al., 2009). We therefore hypothesize that astrocytic end-foot degeneration is a common pathological entity in VCID disorders. Future studies will test this hypothesis in other VCID models and human samples.

Acknowledgments

Research reported in this manuscript was funded by fellowship F31NS092202 (EMW) and grant 1RO1NS079637 (DMW) from the National Institutes of Health. The content is solely the responsibility of the authors and does not necessarily represent the official views of the National Institutes of Health.

References

Alamed J, Wilcock DM, Diamond DM, Gordon MN, Morgan D. Two-day radial-arm water maze learning and memory task; robust resolution of amyloid-related memory deficits in transgenic mice. Nature protocols. 2006; 1:1671–1679. [PubMed: 17487150]

Amiry-Moghaddam M, Frydenlund DS, Ottersen OP. Anchoring of aquaporin-4 in brain: molecular mechanisms and implications for the physiology and pathophysiology of water transport. Neuroscience. 2004a; 129:999–1010. [PubMed: 15561415]

Amiry-Moghaddam M, Otsuka T, Hurn PD, Traystman RJ, Haug FM, Froehner SC, Adams ME, Neely JD, Agre P, Ottersen OP, Bhardwaj A. An alpha-syntrophin-dependent pool of AQP4 in astroglial end-feet confers bidirectional water flow between blood and brain. Proc Natl Acad Sci U S A. 2003; 100:2106–2111. [PubMed: 12578959]

Amiry-Moghaddam M, Xue R, Haug FM, Neely JD, Bhardwaj A, Agre P, Adams ME, Froehner SC, Mori S, Ottersen OP. Alpha-syntrophin deletion removes the perivascular but not endothelial pool of aquaporin-4 at the blood-brain barrier and delays the development of brain edema in an experimental model of acute hyponatremia. FASEB J. 2004b; 18:542–544. [PubMed: 14734638]

Bay V, Butt AM. Relationship between glial potassium regulation and axon excitability: a role for glial Kir4.1 channels. Glia. 2012; 60:651–660. [PubMed: 22290828]

Beydoun MA, Beydoun HA, Gamaldo AA, Teel A, Zonderman AB, Wang Y. Epidemiologic studies of modifiable factors associated with cognition and dementia: systematic review and meta-analysis. BMC public health. 2014; 14:643. [PubMed: 24962204]

Bowler JV, Munoz DG, Merskey H, Hachinski V. Fallacies in the pathological confirmation of the diagnosis of Alzheimer's disease. Journal of neurology, neurosurgery, and psychiatry. 1998; 64:18–24.

Butt AM, Kalsi A. Inwardly rectifying potassium channels (Kir) in central nervous system glia: a special role for Kir4.1 in glial functions. Journal of cellular and molecular medicine. 2006; 10:33–44. [PubMed: 16563220]

Camassa LM, Lunde LK, Hoddevik EH, Stensland M, Boldt HB, De Souza GA, Ottersen OP, Amiry-Moghaddam M. Mechanisms underlying AQP4 accumulation in astrocyte endfeet. Glia. 2015

Chakrabarti S, Zee JM, Patel KD. Regulation of matrix metalloproteinase-9 (MMP-9) in TNF-stimulated neutrophils: novel pathways for tertiary granule release. J Leukoc Biol. 2006; 79:214–222. [PubMed: 16275891]

Clarke R, Smith AD, Jobst KA, Refsum H, Sutton L, Ueland PM. Folate, vitamin B12, and serum total homocysteine levels in confirmed Alzheimer disease. Arch Neurol. 1998; 55:1449–1455. [PubMed: 9823829]

Connors NC, Kofuji P. Dystrophin Dp71 is critical for the clustered localization of potassium channels in retinal glial cells. J Neurosci. 2002; 22:4321–4327. [PubMed: 12040037]

Czerniawski J, Miyashita T, Lewandowski G, Guzowski JF. Systemic lipopolysaccharide administration impairs retrieval of context-object discrimination, but not spatial, memory: Evidence for selective disruption of specific hippocampus-dependent memory functions during acute neuroinflammation. Brain Behav Immun. 2015; 44:159–166. [PubMed: 25451612]

Dunn KM, Nelson MT. Potassium channels and neurovascular coupling. Circ J. 2010; 74:608–616. [PubMed: 20234102]

Farr H, David T. Models of neurovascular coupling via potassium and EET signalling. J Theor Biol. 2011; 286:13–23. [PubMed: 21781976]

Gondo A, Shinotsuka T, Morita A, Abe Y, Yasui M, Nuriya M. Sustained down-regulation of beta-dystroglycan and associated dysfunctions of astrocytic endfeet in epileptic cerebral cortex. J Biol Chem. 2014; 289:30279–30288. [PubMed: 25228692]

Haj-Yasein NN, Jensen V, Vindedal GF, Gundersen GA, Klungland A, Ottersen OP, Hvalby O, Nagelhus EA. Evidence that compromised K+ spatial buffering contributes to the epileptogenic effect of mutations in the human Kir4.1 gene (KCNJ10). Glia. 2011; 59:1635–1642. [PubMed: 21748805]

Kammoun S, Gold G, Bouras C, Giannakopoulos P, McGee W, Herrmann F, Michel JP. Immediate causes of death of demented and non-demented elderly. Acta Neurol Scand Suppl. 2000; 176:96–99. [PubMed: 11261812]

Klein T, Bischoff R. Physiology and pathophysiology of matrix metalloproteases. Amino Acids. 2011; 41:271–290. [PubMed: 20640864]

Langa KM, Foster NL, Larson EB. Mixed dementia: emerging concepts and therapeutic implications. JAMA: the journal of the American Medical Association. 2004; 292:2901–2908. [PubMed: 15598922]

Larsen BR, MacAulay N. Kir4.1-mediated spatial buffering of K(+): experimental challenges in determination of its temporal and quantitative contribution to K(+) clearance in the brain. Channels (Austin). 2014; 8:544–550. [PubMed: 25483287]

Levine DA, Langa KM. Vascular cognitive impairment: disease mechanisms and therapeutic implications. Neurotherapeutics: the journal of the American Society for Experimental NeuroTherapeutics. 2011; 8:361–373. [PubMed: 21556678]

Livak KJ, Schmittgen TD. Analysis of relative gene expression data using real-time quantitative PCR and the 2(−Delta Delta C(T)) Method. Methods. 2001; 25:402–408. [PubMed: 11846609]

Loesch M, Zhi HY, Hou SW, Qi XM, Li RS, Basir Z, Iftner T, Cuenda A, Chen G. p38gamma MAPK cooperates with c-Jun in trans-activating matrix metalloproteinase 9. J Biol Chem. 2010; 285:15149–15158. [PubMed: 20231272]

Metea MR, Kofuji P, Newman EA. Neurovascular coupling is not mediated by potassium siphoning from glial cells. J Neurosci. 2007; 27:2468–2471. [PubMed: 17344384]

Michaluk P, Kolodziej L, Mioduszewska B, Wilczynski GM, Dzwonek J, Jaworski J, Gorecki DC, Ottersen OP, Kaczmarek L. Beta-dystroglycan as a target for MMP-9, in response to enhanced neuronal activity. J Biol Chem. 2007; 282:16036–16041. [PubMed: 17426029]

Newman EA, Frambach DA, Odette LL. Control of extracellular potassium levels by retinal glial cell K+ siphoning. Science. 1984; 225:1174–1175. [PubMed: 6474173]

Noell S, Wolburg-Buchholz K, Mack AF, Beedle AM, Satz JS, Campbell KP, Wolburg H, Fallier-Becker P. Evidence for a role of dystroglycan regulating the membrane architecture of astroglial endfeet. Eur J Neurosci. 2011; 33:2179–2186. [PubMed: 21501259]

Price DL, Ludwig JW, Mi H, Schwarz TL, Ellisman MH. Distribution of rSlo Ca2+-activated K+ channels in rat astrocyte perivascular endfeet. Brain Res. 2002; 956:183–193. [PubMed: 12445685]

Refsum H, Ueland PM, Nygard O, Vollset SE. Homocysteine and cardiovascular disease. Annu Rev Med. 1998; 49:31–62. [PubMed: 9509248]

Semmler A, Frisch C, Debeir T, Ramanathan M, Okulla T, Klockgether T, Heneka MT. Long-term cognitive impairment, neuronal loss and reduced cortical cholinergic innervation after recovery from sepsis in a rodent model. Exp Neurol. 2007; 204:733–740. [PubMed: 17306796]

Simard M, Nedergaard M. The neurobiology of glia in the context of water and ion homeostasis. Neuroscience. 2004; 129:877–896. [PubMed: 15561405]

Snyder HM, Corriveau RA, Craft S, Faber JE, Greenberg SM, Knopman D, Lamb BT, Montine TJ, Nedergaard M, Schaffer CB, Schneider JA, Wellington C, Wilcock DM, Zipfel GJ, Zlokovic B, Bain LJ, Bosetti F, Galis ZS, Koroshetz W, Carrillo MC. Vascular contributions to cognitive impairment and dementia including Alzheimer's disease. Alzheimer's & dementia: the journal of the Alzheimer's Association. 2015; 11:710–717.

Strohschein S, Huttmann K, Gabriel S, Binder DK, Heinemann U, Steinhauser C. Impact of aquaporin-4 channels on K+ buffering and gap junction coupling in the hippocampus. Glia. 2011; 59:973–980. [PubMed: 21446052]

Sudduth TL, Powell DK, Smith CD, Greenstein A, Wilcock DM. Induction of hyperhomocysteinemia models vascular dementia by induction of cerebral microhemorrhages and neuroinflammation.

Journal of cerebral blood flow and metabolism: official journal of the International Society of Cerebral Blood Flow and Metabolism. 2013

Sudduth TL, Weekman EM, Brothers HM, Braun K, Wilcock DM. beta-amyloid deposition is shifted to the vasculature and memory impairment is exacerbated when hyperhomocysteinemia is induced in APP/PS1 transgenic mice. Alzheimer's research & therapy. 2014; 6:32.

Sun J, Zhang S, Zhang X, Zhang X, Dong H, Qian Y. IL-17A is implicated in lipopolysaccharide-induced neuroinflammation and cognitive impairment in aged rats via microglial activation. J Neuroinflammation. 2015; 12:165. [PubMed: 26373740]

Troen AM, Shea-Budgell M, Shukitt-Hale B, Smith DE, Selhub J, Rosenberg IH. B-vitamin deficiency causes hyperhomocysteinemia and vascular cognitive impairment in mice. Proc Natl Acad Sci U S A. 2008; 105:12474–12479. [PubMed: 18711131]

Wallraff A, Kohling R, Heinemann U, Theis M, Willecke K, Steinhauser C. The impact of astrocytic gap junctional coupling on potassium buffering in the hippocampus. The Journal of neuroscience: the official journal of the Society for Neuroscience. 2006; 26:5438–5447. [PubMed: 16707796]

Wilcock DM, Lewis MR, Van Nostrand WE, Davis J, Previti ML, Gharkholonarehe N, Vitek MP, Colton CA. Progression of amyloid pathology to Alzheimer's disease pathology in an amyloid precursor protein transgenic mouse model by removal of nitric oxide synthase 2. J Neurosci. 2008; 28:1537–1545. [PubMed: 18272675]

Wilcock DM, Rojiani A, Rosenthal A, Subbarao S, Freeman MJ, Gordon MN, Morgan D. Passive immunotherapy against Abeta in aged APP-transgenic mice reverses cognitive deficits and depletes parenchymal amyloid deposits in spite of increased vascular amyloid and microhemorrhage. J Neuroinflammation. 2004; 1:24. [PubMed: 15588287]

Wilcock DM, Vitek MP, Colton CA. Vascular amyloid alters astrocytic water and potassium channels in mouse models and humans with Alzheimer's disease. Neuroscience. 2009; 159:1055–1069. [PubMed: 19356689]

Witthoft A, Filosa JA, Karniadakis GE. Potassium buffering in the neurovascular unit: models and sensitivity analysis. Biophys J. 2013; 105:2046–2054. [PubMed: 24209849]

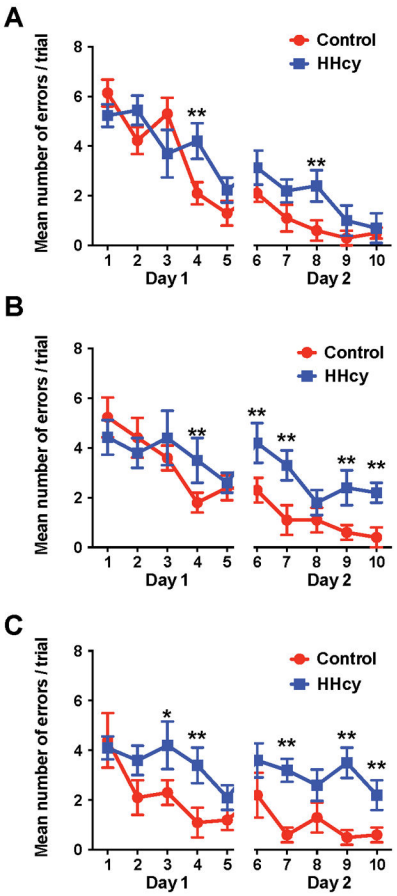

Figure 1. The two-day radial arm water maze task shows progressive cognitive deficits in HHcy mice relative to mice on control diet

Panels A–C show mean number of errors per trial for mice receiving either control diet (red lines) or HHcy-inducing diet (blue lines). Each block number is the average of errors for three individual trials. Individual groups of mice were tested after being on diet for 6 weeks (A), 10 weeks (B), and 14 weeks (C). * indicates $P<0.05$; ** indicates $P<0.01$ for the given block comparison between mice on control diet for the same time.

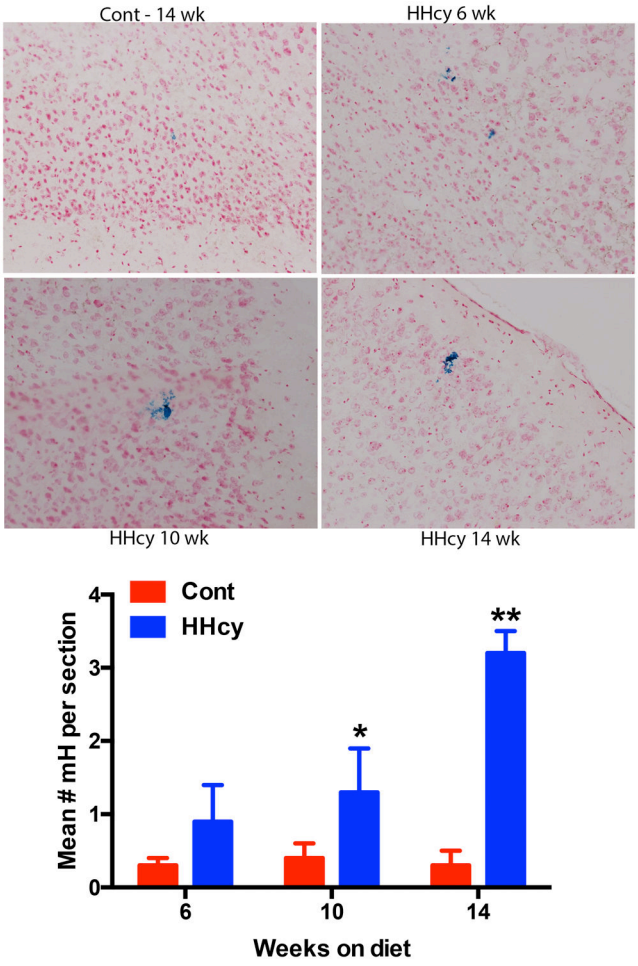

Figure 2. Microhemorrhages are increased in number after 10 and 14 weeks on HHcy inducing diet

The images show representative Prussian blue positive microhemorrhages from either mice on control diet for 14 weeks, or mice on HHcy inducing diet for 6, 10 and 14 weeks. Microhemorrhages are shown as blue staining on the neutral red counterstained background. The graph shows the mean number of microhemorrhages per section for each group of animals. The mean is calculated from counts of 16 sections per animal. * indicates $P<0.05$; ** indicates $P<0.01$ when compared to mice on control diet for the same time.

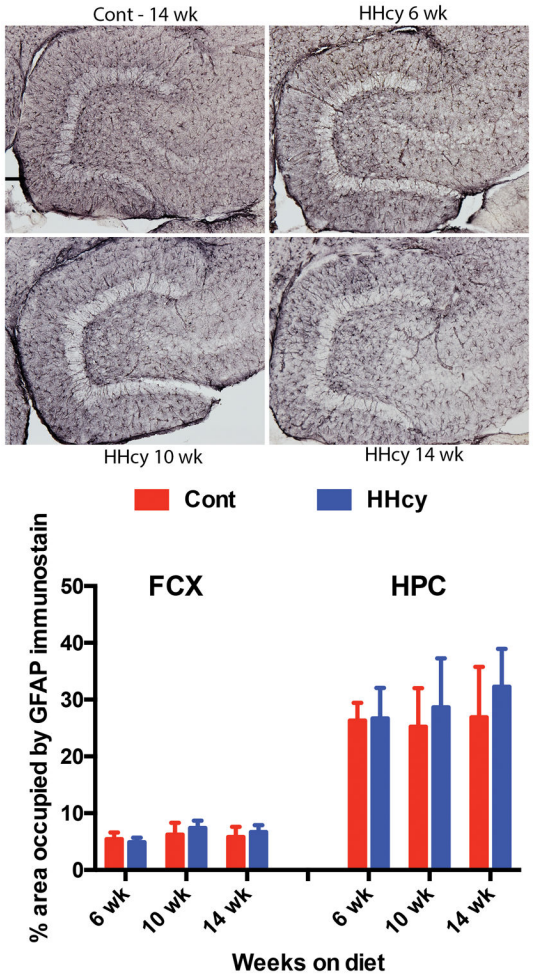

Figure 3. HHcy does not induce a significant astrogliosis in the brain

The images show representative GFAP immunohistochemistry in the dentate gyrus of the hippocampus from either mice on control diet for 14 weeks, or mice on HHcy inducing diet for 6, 10 and 14 weeks. The graph shows percent area occupied by GFAP-positive immunostaining in the frontal cortex and hippocampus of mice receiving control diet (red bars) or HHcy-inducing diet (blue bars).

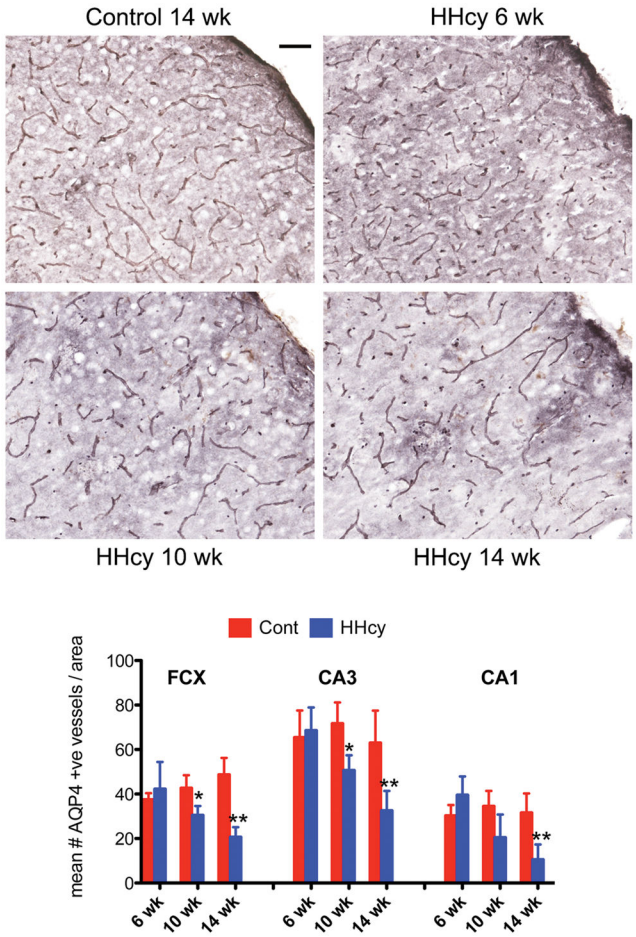

Figure 4. Astrocytic end-foot expression of AQP4 is significantly reduced following 10 and 14 weeks of HHcy-inducing diet

The images show representative AQP4 immunohistochemistry in the frontal cortex from either mice on control diet for 14 weeks, or mice on HHcy inducing diet for 6, 10 and 14 weeks. The graph shows mean number of AQP4-positive vessels in the frontal cortex (FCX) and hippocampus (CA3 and CA1 regions) of mice receiving control diet (red bars) or HHcy-inducing diet (blue bars). * indicates $P<0.05$; ** indicates $P<0.01$ when compared to mice on control diet for the same time.

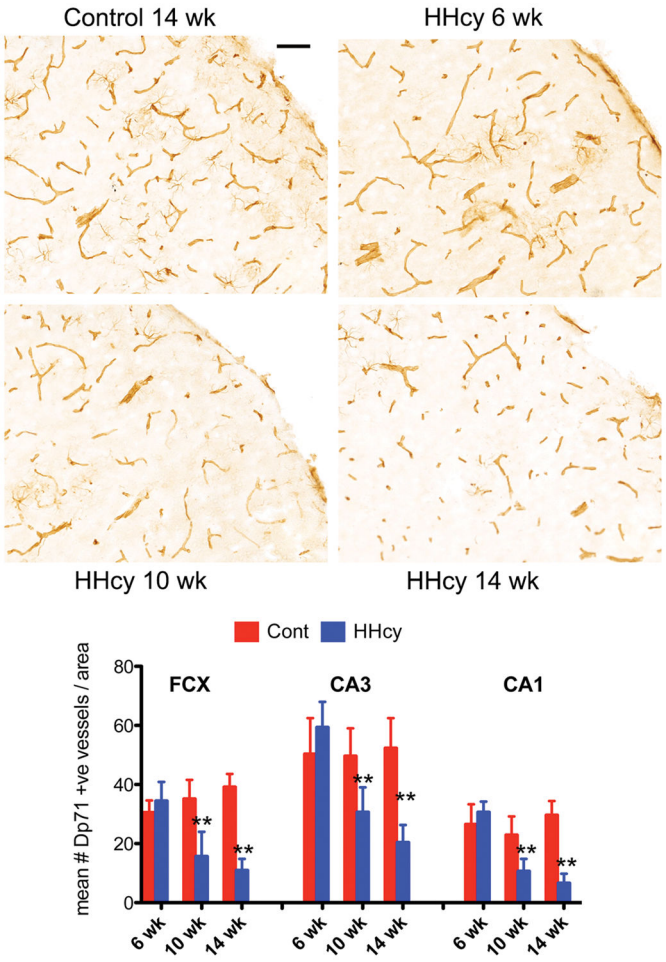

Figure 5. Astrocytic end-foot expression of Dp71 is significantly reduced following 10 and 14 weeks of HHcy-inducing diet

The images show representative Dp71 immunohistochemistry in the frontal cortex from either mice on control diet for 14 weeks, or mice on HHcy inducing diet for 6, 10 and 14 weeks. The graph shows mean number of Dp71-positive vessels in the frontal cortex (FCX) and hippocampus (CA3 and CA1 regions) of mice receiving control diet (red bars) or HHcy-inducing diet (blue bars). ** indicates $P<0.01$ when compared to mice on control diet for the same time.

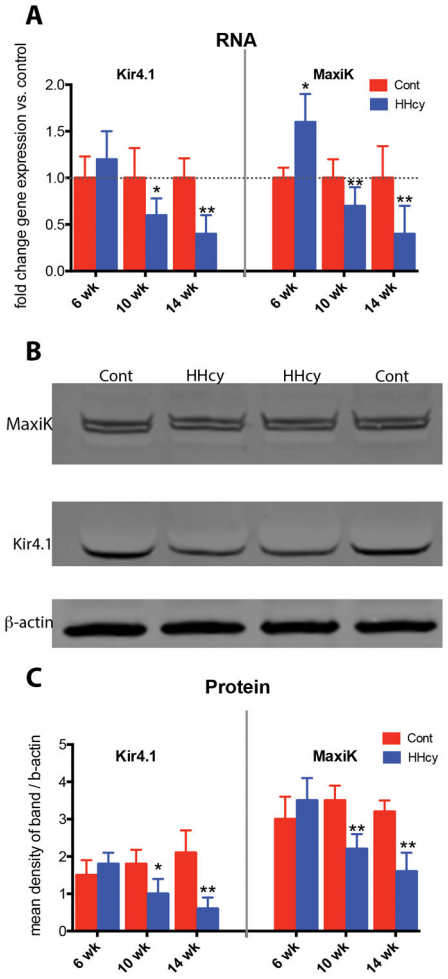

Figure 6. Expression of Kir4.1 and MaxiK is decreased after 10 and 14 weeks of HHcy induction

The hippocampus was used for gene expression analysis and the frontal cortex for the protein analysis. The graph in A shows fold-change from the mice on control diet of Kir4.1 and MaxiK gene expression analysis by qPCR. The image in B show representative images of Western blots for MaxiK, Kir4.1 and b-actin. These are the same samples for all 3 images. The graph in C shows the quantification of band density for Kir4.1 and MaxiK normalized to the density of the corresponding b-actin band. Each bar is the average of all animals for each time-point. For graphs, * indicates $P<0.05$; ** indicates $P<0.01$ when compared to mice on control diet for the same time.

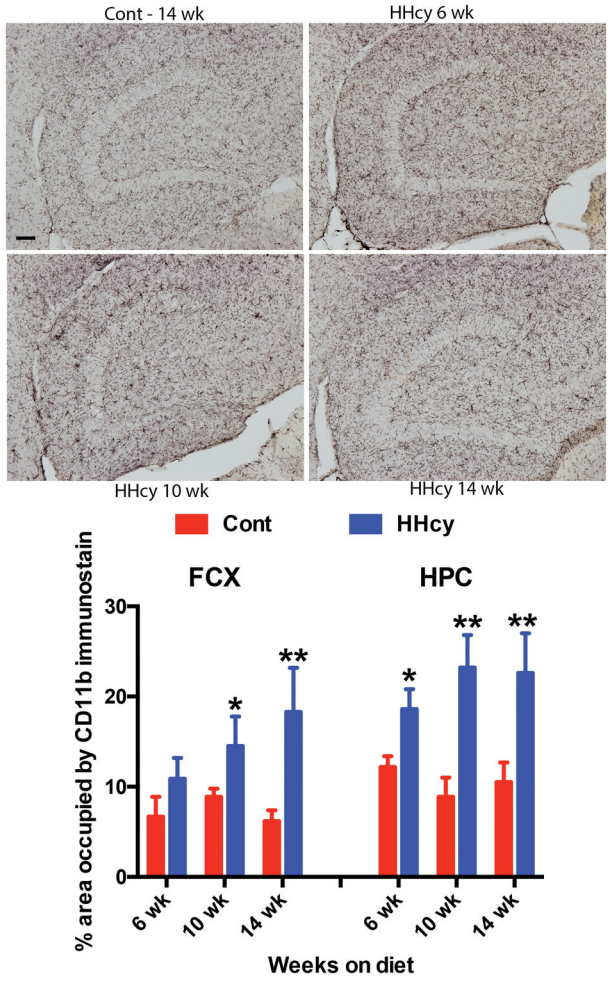

Figure 7. HHcy activates microglia at all time-points examined

The images show representative CD11b immunohistochemistry in the dentate gyrus of the hippocampus from either mice on control diet for 14 weeks, or mice on HHcy inducing diet for 6, 10 and 14 weeks. The graph shows percent area occupied by CD11b-positive immunostaining in the frontal cortex and hippocampus of mice receiving control diet (red bars) or HHcy-inducing diet (blue bars). * indicates $P<0.05$; ** indicates $P<0.01$ when compared to mice on control diet for the same time.

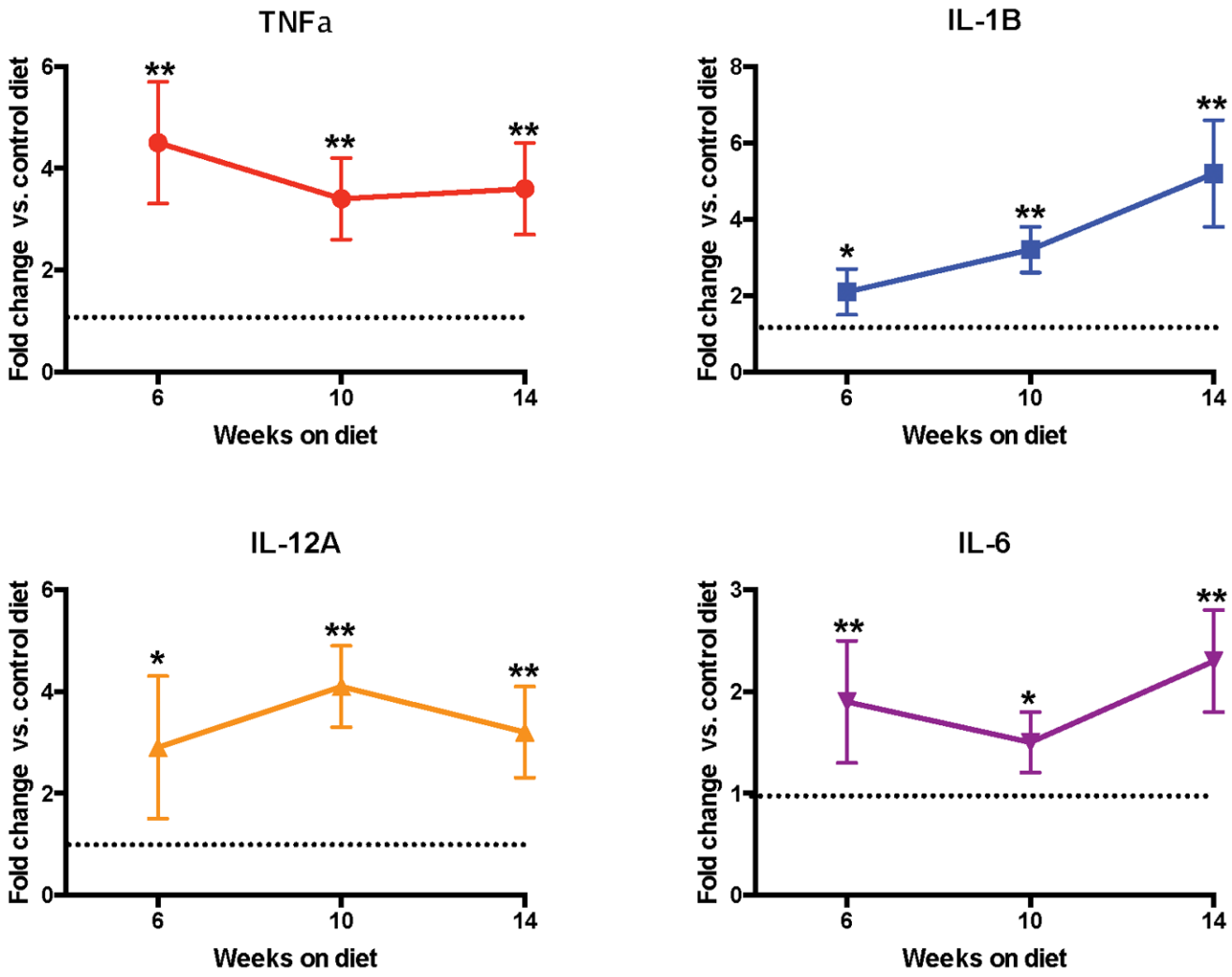

Figure 8. Pro-inflammatory mediators are increased by HHcy

qPCR analysis for TNFα, IL-1β, IL-12A and IL-6 was performed and the graphs show the fold change at 6, 10 and 14 weeks relative to mice on control diet for the same amount of time. * indicates P<0.05; ** indicates P<0.01 when comparing HHcy mice to mice on control diet for the same time.